Available online at www.sciencedirect.com
ScienceDirect
Catalysis Today 126 (2007) 248–255
CATALYSIS TODAY
www.elsevier.com/locate/cattod

In situ thermo-Raman study of titanium oxide nanotubes

M.A. Cortés-Jácome, G. Ferrat-Torres, L.F. Flores Ortiz, C. Angeles-Chávez, E. López-Salinas, J. Escobar, M.L. Mosqueira, J.A. Toledo-Antonio *

Instituto Méxicano del Petróleo, Prog. de Ingeniería Molecular, Eje Central Lázaro Cárdenas # 152, 07730 México, D.F., México

Available online 23 March 2007

Abstract

Titania nanotubes were obtained by alkaline hydrothermal treatment of anatase powder at 100 °C followed by washing with an HCl aqueous solution. The resulting nanotubes were composed by one or two structural layers with an interlayer space *ca*. 0.826 nm, showing inner and outer diameters of around 5 and 10 nm, respectively. The walls of the nanotubes were composed of layers of an orthorhombic structure with lattice parameters (in nm) $a = 0.301$, $b = 0.382$ and $c = 0.826$. The thermal stability of the structure depended on the annealing conditions. Under inert atmosphere, the structure transformed into anatase at 250 °C, while under oxidizing conditions the structure was more stable, where the transition started at 400 °C. During annealing, the nanotubular structure releases hydroxyls and Ti^{4+} cations are self-reduced into Ti^{3+}generating a non-stoichiometric anatase phase, which collapse the initial nanotubular morphology. The self-reduction is enhanced when annealing is carried out in inert atmosphere in comparison with that in air, producing highly oxygen-deficient anatase.

Keywords: Annealing; Atmosphere; Oxygen-deficient anatase

1. Introduction

Titanium oxides have attracted considerable attention because their multiple potential applications. They have been used as semiconductor materials in the construction of electronics devices [1], in the manufacturing of pigments and coatings [2], in solar cells [3], in sensors [4], in cosmetics, as catalysts support in several processes [5–8], as photo-catalysts in the degradation of organic compounds in environmental protection process [9], etc. Among others, titanium oxide exists in three most common crystalline phases: anatase, rutile and brookite [10]. Anatase and rutile ones have a tetragonal crystal structure while brookite is orthorhombic. In these phases, Ti atoms are coordinated to six O atoms in octahedral environment, the main differences between them stemming from the position of the atoms, the lattice parameters, the space groups, etc., which in turn determine the Ti–O bond lengths and the macroscopic properties observed in these materials [11]. Anatase, the phase with the widest scope of applications can be easily obtained through conventional routes using chloride or sulfate as precursors. However, to date anatase or rutile phases have shown limited specific surface area (i.e. lower than 50 m^2/g) limiting their applications where adsorption phenomena are involved such as catalysis.

Much effort has been devoted to refining the preparation and synthesis of anatase with the goal of continuous improvement on its textural and acidic properties. Recent progress has been achieved in the preparation of anatase-based catalysts supports with higher specific areas and increased active phase loadings [5,8,12]. In this regard, a multi-gelation method has been developed by Inoue et al. [5,8,12] obtaining an upgraded titania with high surface area, where the corresponding supported CoMoS hydrotreatment catalysts showed increased activity in light gas oil desulfurization and denitrogenation [8].

Recently, nanotubes of titania have been synthesized through a relatively simple alkaline hydrothermal method, which represent an alternative to increase the specific surface area [13,14]. Accordingly, nanotubes exhibit large internal and external surfaces, along with surface in the vertex and in the interlayer regions that compose the nanotube walls [15,16]. In fact, transformation of titania into nanotubes yields materials with specific surface area as large as 400 m^2/g [17], opening the possibility of using this material as catalyst support in several processes. Recently, we have reported that nanostructured

* Corresponding author. Tel.: +52 55 91 75 8433.
E-mail address: jtoledo@imp.mx (J.A. Toledo-Antonio).

0920-5861/$ – see front matter © 2007 Elsevier B.V. All rights reserved.
doi:10.1016/j.cattod.2007.02.012

CoMoS/titania (i.e., cobalt–molybdenum on titania nanotubes) are twice as active in dibenzothiophene hydrodesulphurization as compared with the corresponding alumina-supported catalyst [18].

Thermal stability of these inorganic oxide nanotubes must be taken into account when applying these materials as catalysts support. In situ thermo-Raman spectroscopy is an effective technique in characterizing phase transformations of bulk oxides. In this work, in situ thermo-Raman spectroscopy was used to study the structural evolution of titania nanotubes and the phase transformations taking place in oxidizing and inert atmospheres. Moreover, samples were characterized by X-ray diffraction, X-ray photoelectron spectroscopy, high resolution transmission electron microscopy and nitrogen physisorption.

2. Experimental

2.1. Preparation of titania nanotubes

Titania with nanotubular morphology was synthesized by hydrothermal treatment of an anatase precursor with crystallite size of 22 nm (as determined by XRD, Fig. 1b). Anatase precursor used in this study was Hombitec K03 from Sachtleben Chemie GmbH. Forty-five grams of TiO_2 anatase powder was suspended in 3 L of an aqueous 10 M NaOH solution and the resulting suspension was placed in a 4 L autoclave. The hydrothermal reaction was conducted at 100, during 48 h under stirring at 200 rpm. Thereafter, the white slurry was filtered and neutralized with a 1 M solution of hydrochloric acid until the pH was lowered to 3.0. The resulting suspension was maintained at this pH overnight under continuous stirring. Then, the material was repeatedly washed with abundant deionized water until it was chloride-free, as tested with silver nitrate solution. The material was then dried at 110 °C overnight yielding a hydrous titania powder with nanotubular morphology.

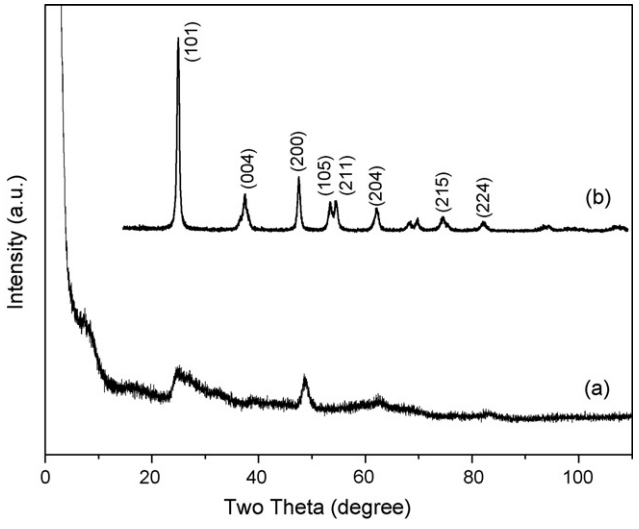

Fig. 1. XRD patterns of product and precursor materials: (a) titania nanotubes at 110 °C; (b) anatase precursor.

2.2. Characterization

2.2.1. X-ray diffraction

X-ray diffraction (XRD) patterns of the samples packed in a glass holder were recorded at room temperature with Cu Kα radiation in a Bruker Advance D-8 diffractometer having theta–theta configuration and a graphite secondary-beam monochromator. Diffraction intensity was measured in the 2θ range between 2° and 110°, with a 2θ step of 0.02° for 8 s per point.

2.2.2. High-resolution transmission electron microscopy

High-resolution transmission electron microscopy (HR-TEM) analyses of the samples were performed in a JEOL 2010F microscope operating at 200 kV and equipped with a Schottky-type field emission gun and an ultrahigh resolution pole piece (Cs = 0.5 mm, point-to-point resolution, 0.190 nm). The samples were ground, suspended in isopropanol at room temperature and dispersed by ultrasonic agitation. Then, an aliquot of the solution was dropped on a 3 mm diameter lacey carbon copper grid. Chemical analysis by X-ray energy dispersive spectroscopy (EDS) was performed in an environmental scanning electron microscope XL30 which has attached an X-ray energy dispersive spectroscope.

2.2.3. Raman spectroscopy

Raman spectra were recorded using an Yvon Jobin Horiba (T64000) spectrometer, equipped with a confocal microscope (Olympus, BX41) with an argon ion laser operating at 514.5 nm at a power level of 10 mW. The spectrometer is equipped with a CCD camera detector. Powdered titania nanotubes were placed in a Linkam cell stage directly adapted to the microscope of the instrument, which provides controlled atmosphere and temperature. The window of the cell was made of glass and was 0.3 mm thick. Thermo-Raman studies were recorded in flowing inert or oxidizing atmosphere in a dynamic thermal process, heating from 25 to 550 °C at a rate of 2 °C/min. The spectra were taken continuously with a 12 s exposure time each 10 °C. A low laser power level of 10 mW was used in order to avoid any heating effect due to laser irradiation.

2.2.4. X-ray photoelectron spectroscopy

X-ray photoelectron spectroscopy (XPS) spectra were recorded on a THERMO-VG SCALAB 250 spectrometer equipped with Al Kα X-ray source (1486.6 eV) and a hemispherical analyzer. The base pressure during the analysis was 10^{-9} torr. The XPS analyses were performed in a static system in samples annealed in situ under inert atmosphere in the heating chamber. The experimental peaks were decomposed into components using mixed Gaussian–Lorentzian functions, non-linear squares fitting algorithm and Shirley-type background subtraction by using XPS Peak Fit software. The binding energies (BE) were referenced to the adventitious carbon C(1s) peak at 284.6 eV. Changes in the Ti 2p signal shape on the samples calcined at different temperatures were analyzed by a curve fitting procedure with doublets endowed

with fixed spectroscopic parameters, but using variable position, full width at half maximum (FWHM) and intensities. The O/Ti atomic ratio was determined from the corresponding peak areas after subtracting the inelastic background and correction of the peak areas by the respective sensitivity factors.

2.2.5. Nitrogen physisorption

BET surface areas, pore volume and pore size distribution were obtained by nitrogen physisorption in an ASAP-2000 analyzer from Micromeritics. Dried samples were outgassed at 110 °C whereas for the annealing samples this pretreatment was carried out at 300 °C.

3. Results and discussion

The XRD pattern of the TiO_2 (anatase phase) used as starting material for the synthesis of titania nanotubes is presented in Fig. 1b. The crystallite size of the anatase precursor was around 22.0 nm and its specific surface area, as determined by nitrogen physisorption by BET method, was 101 m^2/g. After alkaline hydrothermal treatment at 100 °C, the anatase phase was transformed into titania nanotubes; its corresponding XRD patterns showing only three broad peaks at $2\theta = 7.5$, 24.5 and 48.5, as shown in Fig. 1a. No XRD peaks corresponding to anatase phase were observed in the sample obtained at 100 °C, suggesting that all the anatase nanoparticles were transformed into nanotubes, as confirmed by HRTEM (see Fig. 2).

Accordingly, the peaks in the XRD pattern (Fig. 1a) have been related to hydrogen titanate of general formula $H_2Ti_nO_{2n+1}$, where the peaks are assigned to reflections (0 0 2), (1 1 0) and (0 2 0) of the stepped monoclinic structure with $n = 3$ [19,20]. The lattice parameter suggested for this structure are $a = 1.603$ nm, $b = 0.375$ nm and $c = 0.919$ nm. On the other hand, similar XRD peaks have been assigned to $H_2Ti_2O_4(OH)_2$, where peaks indexed as (2 0 0), (1 1 0) and (0 2 0) planes of an orthorhombic structure [21], having lattice parameters of $a = 1.926$ nm, $b = 0.378$ nm and $c = 0.3$ nm were identified. Another possible approximation to explain the structure has been done by Sasaki et al. [22,23]. They assumed a Lepidocrocite-type structure with orthorhombic symmetry with the general formula: $H_xTi_{2-x/4}\square_{x/4}O_4{\cdot}H_2O$, where $\square$ is a Ti vacancy and the peaks were assigned to (0 2 0), (1 1 0), (1 3 0), (2 0 0) and (0 0 2) planes. The corresponding lattice parameters were $a = 0.3783$ nm, $b = 1.8735$ nm and $c = 0.2978$ nm.

Given the many discrepancies in the structure of titania nanotubes, an HR-TEM approach was applied in order to determine the structure and lattice parameters, due to complexity to determine the structure by XRD and Rietveld analysis. Typical TEM images of the as-made hydrous titania showed that all the samples contain mainly tubular structure. On the other hand, unreacted material was not observed, suggesting a high yield and purity of nanotubes (see Fig. 2), in agreement with our XRD results. At this mild hydrothermal treatment, homogeneous nanotubular structures were obtained with little dispersion in their diameters. The inner diameter was around 5 nm whereas outer diameters of about 8–10 nm could be observed (see Fig. 3). The dark contrast parallel fringes are regarded as the layers of the walls. Then, the nanotubes are composed by one or two structural layers with an interlayer spacing approximately of 0.7–0.8 nm. The length of the nanotubes varied between 100 and 500 nm.

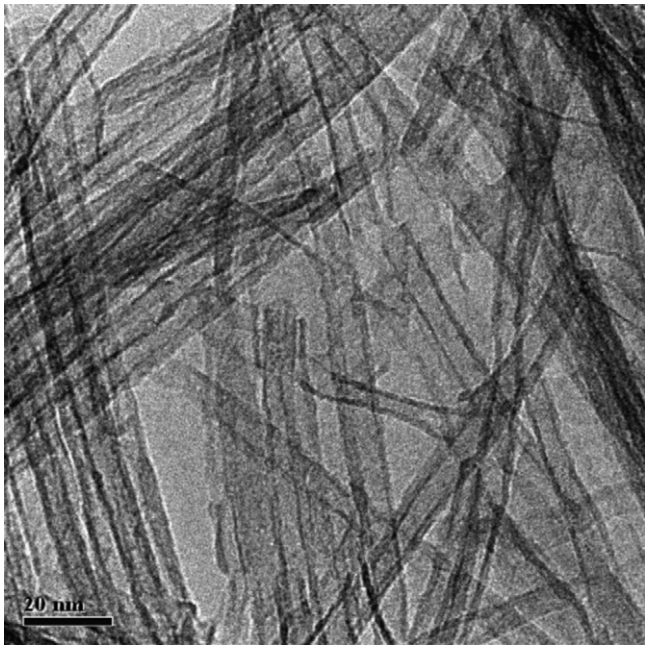

Fig. 2. Bright field TEM micrograph of titania nanotubes dried at 110 °C.

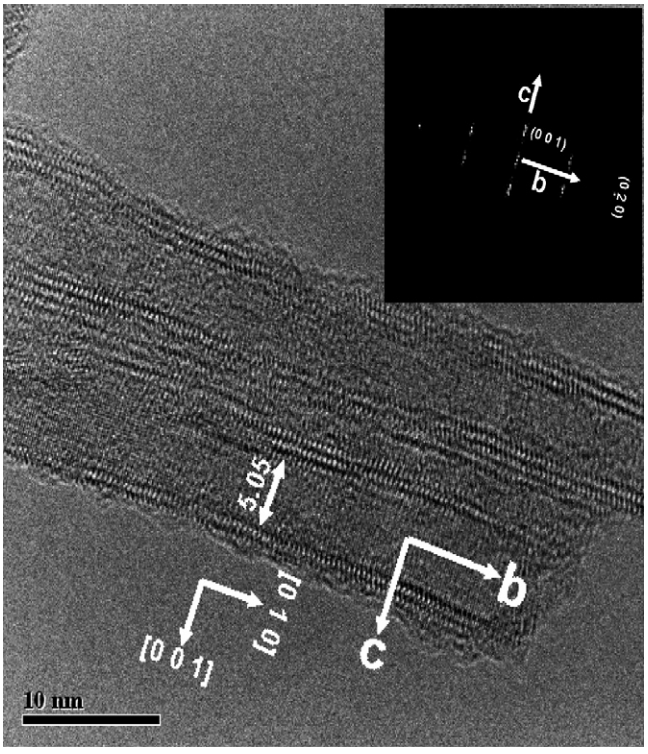

Fig. 3. HR-TEM image showing the crystalline structure of the nanotubes. Inset: FFT pattern showing the main spot generated by the plane in the HRTEM image of a nanotube. The *b*- and *c*-axis are perpendicular between them.

Analyzing several HR-TEM images obtained at different orientations of the nanotubes it was determined that the structured suggested by the analysis is close to an orthorhombic one. These measurements were obtained from reflections observed in the cross-section and along the growth axis of the nanotubes. So, a typical FFT pattern obtained from the HRTEM image (see Fig. 3) shows characteristic spots with a *d*-spacing of 0.826 nm, named as (0 0 1) plane, which represent the interplanar spacing parallel to the length of the nanotubes. Accordingly, we propose that the layered structure of the nanotubes could be described by an orthorrombic symmetry in which each layer is spaced by 0.826 nm, representing a unit cell in the *c*-axis. The interplanar spacing perpendicular to the nanotube axis represented by the most distant spots in FFT pattern (inset in Fig. 3) has a *d*-spacing of 0.191 nm and correspond to the (0 2 0) planes. These planes represent a half of the unit cell in the *b*-axis, therefore the parameter *b* is approximately 0.382 nm. The parameter *a* was obtained analyzing another HR-TEM image and the value measured was 0.301 nm. The FFT patterns were similar to the ED patterns reported for a Lepidocrocite-type structure [22,23]. In this case, an orthorhombic structure with lattice parameters $a = 0.3786$ nm, $b = 1.8375$ nm and $c = 0.2978$ nm was reported, herein the layers of the nanotubular walls are staked along *b*-axis. However, our nanotubes have *d*-spacing that cannot be indexed to this structure. On the other hand, layered titanates with $H_2Ti_2O_5{\cdot}H_2O$ formula, showing body-centered orthorhombic structure with lattice parameters $a = 1.802$ (3) nm, $b = 0.3784$ (3) nm and $c = 0.2998$ (2) nm have been reported [24]. In this case, the layered structure is staked along the *a*-axis, in which *d*-spacing strongly depend on the amount of exchangeable Li^+ located between the layers. Ion-exchanging of Li^+ by H^+ brings about the orthorhombic symmetry change from a C-base centered to a body-centered lattice assuming a slip of middle TiO_6 octahedra layers along *c*-axis with respect to top and bottom octahedra layers [24]. This assumption give rise to a unit cell twice the $d_{(2\,0\,0)}$ spacing composed by at least three TiO_2 octahedra layers. The later structure has been used to explain lattice features observed in titania nanotubes assuming a stoichiometric $Na_2Ti_2O_4(OH)_2$ or $H_2Ti_2O_4(OH)_2$ formulae, the later being the protonic salt of $H_2Ti_2O_5{\cdot}H_2O$ [21]. In fact, by assuming an orthorhombic symmetry of lepidocrocite type structure described by the *Immm* space group geometry [25], atoms positions of $H_2Ti_2O_5{\cdot}H_2O$ with nanotubular morphology were determined [26].

In the present study, we propose that the structure of the layer of nanotubes is described by orthorhombic symmetry with lattice parameters $a = 0.301$ nm, $b = 0.382$ nm and a larger $c = 0.826$ nm. Then, our nanotubes were grown along *b*-axis and the layered structure of the nantoubes was staked along *c*-axis with an interlayer space of 0.826 nm. By analyzing several HRTEM images, several regions of nanotube walls are composed by two structural layers of TiO_6 octahedra. If the mechanism of titania nanotubes were the exfoliation and rolling up of individual layers of flat titanates [25], it is not viable to assume certain degree of slip of the TiO_6 octahedral layers respect to each other. Then, the orthorhombic symmetry of titania nanotubes can be represented by a *Pmmn* space group in which the unit cell along *c*-axis is composed by two TiO_6 octahedra layers with a $d_{(0\,0\,2)}$ spacing of 0.826 nm.

Raman spectra of titania nanotubes after acid treatment and washing with deionized water until total chloride elimination (H-TiO_x) in Fig. 4(b) are made up of three main characteristic bands at 278, 450 and 700 cm^{-1}, and other less intense bands at 192, 380, 825 and 903 cm^{-1}. Anatase active modes at 144, 200, 400, 505, 640 and 796 cm^{-1} were not detected, corroborating complete transformation of the anatase into nanotubular TiO_2. Notwithstanding, the exact assignment of the bands in the Raman spectra of TiO_2 nanotubes is still a matter of debate. Recently, Ma et al. [22,23] reported broad bands at 145,195, 280, 450, 640, 700, and 920 cm^{-1} for similar nanotubes. Evidently, the peaks at 145, 195 and 640 cm^{-1} correspond to the active modes of anatase phase suggesting a mixture of TiO_2 phases, that is, anatase and nanotubular titanates were present. Other recent studies reported Raman bands at 280, 448, 668 and 917 cm^{-1} for titanate nanotubes [27–30] which nearly correspond to the vibrating bands observed in our sample. According to these studies, the bands at 450 and 668 cm^{-1} were assigned to a Ti–O–Ti vibration and the band at 917 cm^{-1} was related to Ti–O–Na vibrations in the interlayer regions of the nanotubes walls [30]. However, in our Raman spectra of the nanotubes, the vibrating band at 665 cm^{-1} is shifted to 700 cm^{-1} and the peak at 917 cm^{-1} was not clearly detected. Since Na^+ ions content (as detected by EDS analysis of our sample) was low (2 wt%), the vibrating band around 917 cm^{-1} assigned to Ti–O–Na vibrations practically disappeared. As a comparison, the Raman spectra of the sample before neutralization with hydrochloric acid (Na–TiO_x) are presented in Fig. 4(a). Practically all the bands remained unchanged, the peaks at 665 and 903 cm^{-1} became more evident suggesting that both are related to the vibration of Ti–O–Na. After acid and

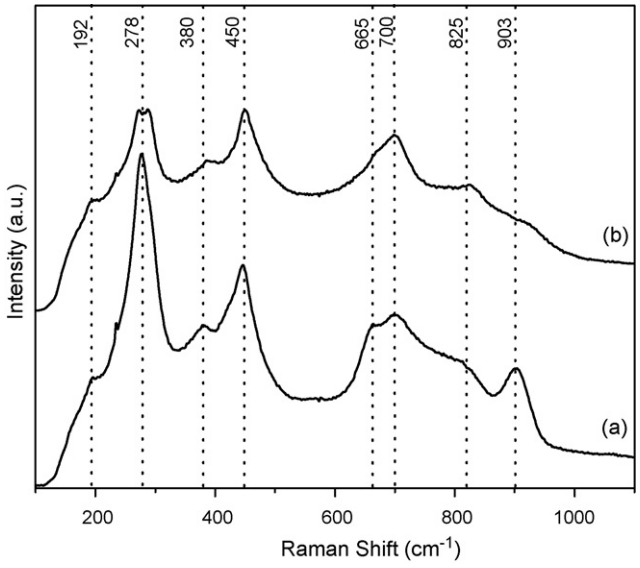

Fig. 4. Raman spectra of: (a) sample before neutralizing with aqueous hydrochloric acid (Na-TiO_x), (b) titania nanotubes after washing with deionized water (H-TiO_x).

washing treatment, Na^+ ions were exchanged by H^+ ions and these bands are not clearly evident.

In situ thermo-Raman studies of titania nanotubes in nitrogen and air atmosphere are presented in Figs. 5 and 6, respectively. Raman spectra taken at room temperature under either flowing nitrogen or air atmosphere showed three main bands at 280, 450 and 700 cm^{-1}. When temperature increased, the vibrating bands corresponding to the nanotubular structure remained unchanged below 250 °C, in nitrogen and below 400 °C in air atmosphere. Above these temperatures one peak around 159 cm^{-1} appeared, this signal being characteristic of the A_{1g} active mode of Ti–O–Ti in anatase structure. The intensity of this peak increased as temperature rose. These results indicate that the transformation of titania nanotubes into anatase begin at 250 °C when the sample is annealed in nitrogen, whereas the nanotubular structure of titania transformed into anatase at about 400 °C in air.

At higher temperatures the vibrating modes assigned to the nanotubular titania decreased and the vibrating modes of anatase phase became more intense. The vibrating band associated to the A_{1g} mode of anatase structure, generally appears at 144 cm^{-1}. However, the anatase produced during the transformation of titania nanotubes by *in situ* annealing, showed this signal at higher frequencies (i.e., 155 cm^{-1}). A plot of the A_{1g} mode Raman position of the anatase phase *versus* annealing temperature is shown in Fig. 7. When the treatment was carried out in nitrogen, as mentioned above anatase phase formed at lower temperature (i.e., at 250 °C) and the A_{1g} mode vibrate at 152 cm^{-1}. The position of this band increased to 159 cm^{-1} at 290 °C, and thereafter decreased slightly, at the end of the *in situ* thermo-Raman treatment at 550 °C. When practically all the vibrating bands associated to nanotubes transformed into anatase phase, the A_{1g} mode vibrate at 155 cm^{-1}, as indicated in Fig. 7. On the other hand, when

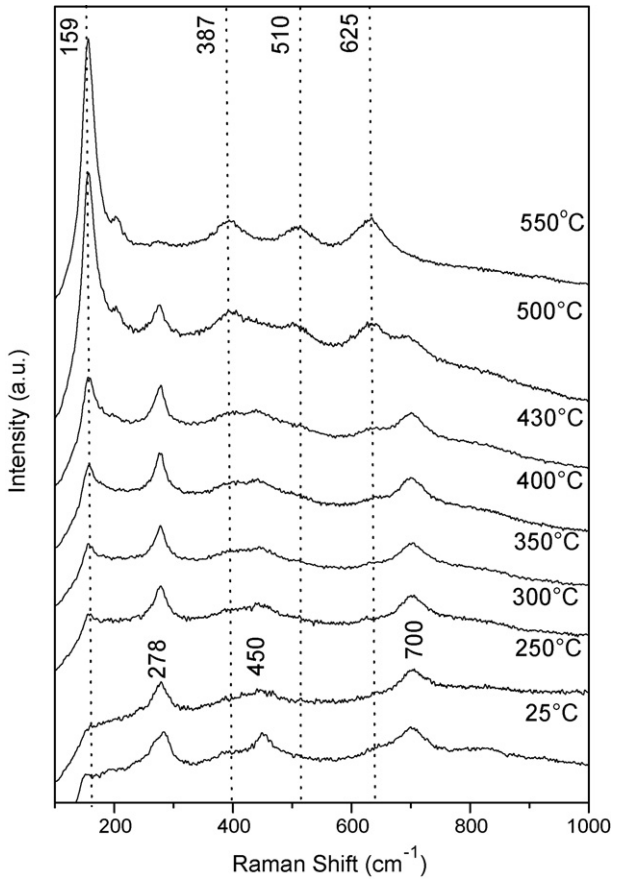

Fig. 5. Thermo-Raman spectra of titania nanotubes in nitrogen atmosphere.

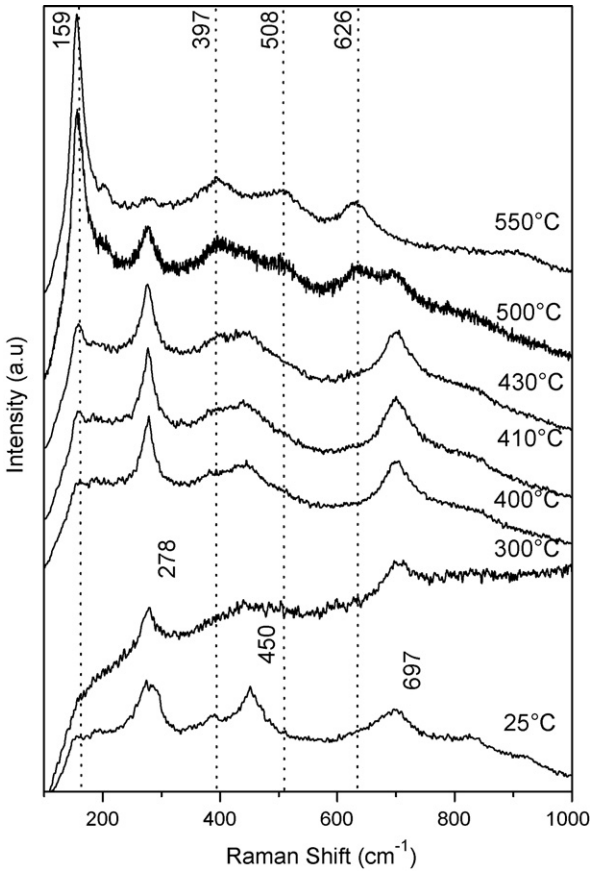

Fig. 6. Thermo-Raman spectra of titania nanotubes in air atmosphere.

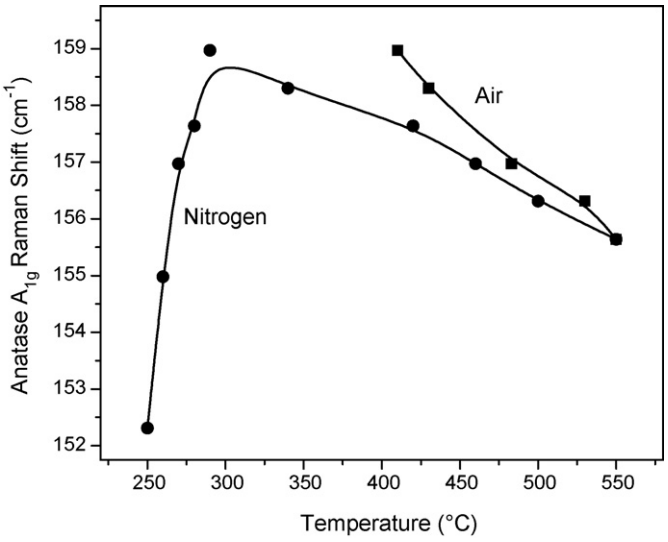

Fig. 7. Plot of Raman anatase $A1_g$ vibration mode *vs.* annealing temperature of titania nanotubes under different atmospheres.

titania nanotubes were heated *in situ* in air, the nanotubular structure showed higher stability than in nitrogen, the A_{1g} vibrating mode of anatase was observable at 159 cm^{-1} (after annealing at 400 °C). The fact that Raman bands shift to lower frequencies with increasing temperature has been attributed to thermal expansion and changes in the population of the vibration energy levels with increasing temperature [31].

The increase in the position of the anatase A_{1g} active mode when heating from 240 to 290 °C in a nitrogen atmosphere can be related to a loss of oxygen and consequent formation of a non-stoichiometric anatase TiO_{2-x}. The loss of oxygen occurs by a self-reduction process during dehydroxilation of the nanotubular structure that reaches a maximum value around 300 °C in inert atmosphere, and at about 400 °C in air. The fact that the position of the A_{1g} Raman band of anatase produced in situ appeared at higher frequencies (155 cm^{-1}) than conventional anatase (144 cm^{-1}) could be attributable to partial reduction of the TiO_2 anatase phase, as confirmed by XPS study (see below). At 550 °C practically all the samples were transformed into anatase and little amount of the sample remained with nanotubular structure. The transformation of the nanotubes into anatase brings about the nanotubular morphology collapse into nanocrystallites, as observed in Fig. 8.

A typical XPS spectrum of an *in situ* heat-treated sample (500 °C, in N_2) is shown in Fig. 9a and b, in the Ti 2p and O 1s regions, respectively. After subtracting the inelastic background, two doublets were necessary to fit the Ti 2p signal. The binding energy (BE) values were assigned to different oxidation states of Ti atoms according to literature data [32–34]. The BE value reported for Ti^{4+} $2p_{3/2}$ is 459.5 eV. This peak shifts to lower energies when the valence state of Ti^{4+} is reduced to Ti^{3+} [35]. Then, the peak around 459.1–459.4 correspond to Ti^{4+} cations, while the small peak used to fit the spectra at the BE values of 457.5–458.1 correspond to reduced Ti^{3+}, suggesting that a small fraction of Ti^{4+} cations are reduced during annealing under N_2. The reduction degree of these cations with the annealing temperature was followed by treating nanotubes samples *in situ* in inert atmosphere at different temperatures. The parameters derived from fitting the XPS curves are presented in Table 1. Noteworthy, even in the dried titania nanotubes a small fraction of Ti^{3+} atoms was observed, which could have been caused by local heating due to the X-ray beam used. When the sample was treated at higher temperature, the population of reduced Ti^{3+} atoms increased giving a Ti^{3+}/Ti^{4+} surface atomic ratio of 0.046 and 0.06 at 300 and 500 °C, respectively.

Concomitantly, the O/Ti surface atomic ratio decreased from 2.48 to 1.89 in the samples treated at 110 and 400 °C, respectively, suggesting a non-stoichiometric surface composition after annealing. In other words, surface oxygen-deficient TiO_{2-x} anatase phase are produced by thermally treating titania nanotubes in dynamic inert atmosphere. Conversely, after annealing at 500 °C the O/Ti surface atomic ratio increased as well as the amount of Ti^{3+}, in comparison to the nanotubes thermally treated at 400 °C. These results supported the assumption that the Raman shift of the A_{1g} vibrating mode (see

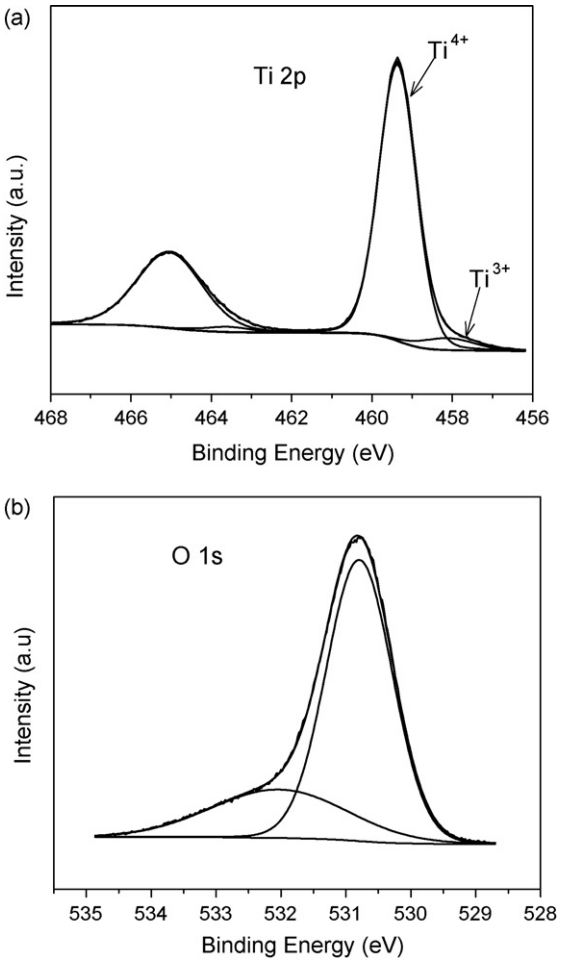

Fig. 9. XPS spectra of titania nanotubes *in situ* treated at 500 °C in N_2 atmosphere: (a) Ti 2p and (b) O 1s region.

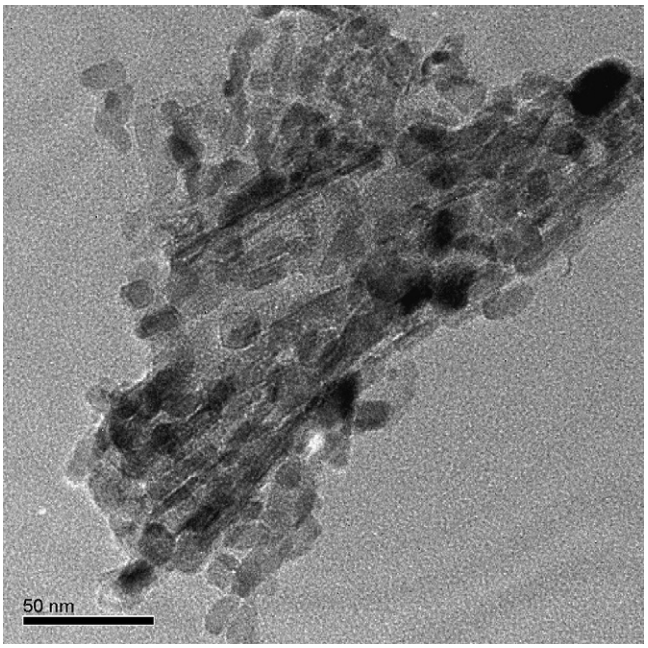

Fig. 8. Bright field TEM image of titania nanotubes after thermo-Raman annealing at 550 °C.

Table 1
XPS parameters of Ti $2p_{3/2}$ and O1s derived from spectra fitting

Annealing temperature (°C)	Assignment	Binding energy (eV)	FWHM[a] (eV)	Surface atomic ratio Ti^{3+}/Ti^{4+}	Surface atomic ratio O/Ti
110	O 1s	530.8	1.3	0.026	2.48
	Ti^{3+} $2p_{3/2}$	457.5	1.2		
	Ti^{4+} $2p_{3/2}$	459.1	1.2		
200	O 1s	530.8	1.2	0.048	2.17
	Ti^{3+} $2p_{3/2}$	457.8	1.2		
	Ti^{4+} $2p_{3/2}$	459.2	1.1		
300	O 1s	530.8	1.2	0.046	1.96
	Ti^{3+} $2p_{3/2}$	458.1	1.4		
	Ti^{4+} $2p_{3/2}$	459.4	1.1		
400	O 1s	530.9	1.2	0.045	1.89
	Ti^{3+} $2p_{3/2}$	458.1	1.4		
	Ti^{4+} $2p_{3/2}$	459.4	1.1		
500	O 1s	530.8	1.2	0.060	1.97
	Ti^{3+} $2p_{3/2}$	458.1	1.6		
	Ti^{4+} $2p_{3/2}$	459.4	1.1		

[a] Full width at half maximum.

above Raman discussion) is due to partially reduced Ti^{3+} atoms or oxygen-deficient anatase phase TiO_{2-x}.

Since the annealing treatment of titania nanotubes brings about titania atoms self-reduction and nanotubular structure collapse by phase transformation from orthorhombic nanotubes into tetragonal anatase nanoparticles, it is interesting to examine how this process affect the textural properties. Nitrogen physisorption isotherms for titania nanotubes treated in nitrogen atmosphere at 100, 300 and 400 °C are shown in Fig. 10. All of them were type IV isotherms from BDDT classification [36], often observed in porous solids. The initial slope of the hysteresis loop reflects porous structure shrinkage caused by the stress change of the condensate during depressurization. The sharp decline in the desorption curve at relative pressure of 0.4–0.6 indicates the internal mesoporosity of the nanotubes. The hysteresis loop shifted towards higher relative pressure as temperature rose, which reflects an increase in average pore size (see inset in Fig. 10). The average pore diameter determined from the desorption branch (see Table 2), nearly corresponded to the internal diameter of the nanotubes as measured from our HRTEM image in Fig. 3.

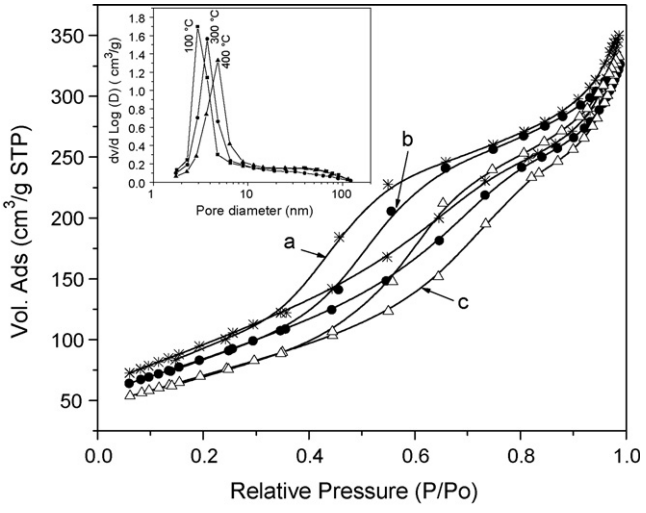

Fig. 10. Nitrogen adsorption–desorption isotherms of titania nanotubes treated in N_2 at (a) 100 °C, (b) 300 °C and (c) 400 °C. Corresponding pore size distribution plots are shown in the inset.

The pore volume of the nanotubular material remained practically constant as pointed out in Table 2. Pore diameter increased from 4.3 nm (in the dried sample) to 5.5 nm, after annealing at 400 °C. On the other hand, surface area decreased from 348 to 256 m^2/g, which could be explained by the gradual collapse of the structural layers of the titania nanotubes. After annealing at 300 °C, pore diameter and pore volume did not vary considerably in comparison with those of the titania nanotubes dried at 110 °C, suggesting that the nanotubular structure remained intact in full agreement with our Raman spectroscopy results (see Fig. 5). After annealing at 400 °C, the pore diameter increased up to 5.5 nm without any pore volume variation, then, pore size increase could be explained by the collapse of the layers of the nanotubes walls. Eventually, the interaction among adjacent octahedra of the nanotubes walls results in a tridimensional growth of tetragonal structure yielding anatase phase domains.

Then, after annealing at 400 °C, titania nanotubes with anatase domains on their walls and highly defective surfaces was obtained, yielding a support with high specific surface area exposing inner and outer surfaces where noble metals or other catalytic active phases could be dispersed to produce enhanced activity heterogeneous catalysts. Nanotubular titania prepared through various methodologies has found interesting applications in various reaction schemes. For instance, Idakieva et al. [37] impregnated Au particles by deposition–precipitation on nanotubes obtained by alkaline hydrotreatment of sol–gel titania, observing higher activity in the water-gas shift reaction than over alumina-supported samples. This behavior, however, was dependent on the nature of the TiO_2 precursor used during nanotube synthesis. The feasibility of taking advantage of the high surface area of nanotubular titania as carrier of sulfided CoMo catalysts intended for the production of ultra clean fuels

Table 2
Textural properties of titania nanotubes annealed at different temperatures under N_2 atmosphere

Annealing temperature (°C)	Surface area (m^2/g)	Total pore volume (cm^3/g)	Average pore diameter (nm)
110	348	0.56	4.3
300	304	0.52	4.5
400	256	0.52	5.5

was recently reported by our group [18], where very high dispersion and sulfidability of impregnated phases were correlated to their striking performance in dibenzothiophene conversion. Also, noble metal nanoparticles of Ag and Au have been deposited in and on nanotubular titania by Ma et al. [38], who considered that the crucial step in obtaining high dispersion of supported particles into the hollow titania cylinders was the internal diffusion of precursor cations, phenomenon that could be enhanced by the confinement effect of the capillary forces.

4. Conclusions

Titania nanotubes were obtained by alkaline hydrothermal treatment of anatase phase at 100 °C. The nanotubes were composed by one or two structural layers with an interlayer space around 0.826 nm, showing inner and outer diameters of 5 and 10 nm, respectively. The walls of the nanotubes are composed of layers of an orthorhombic structure with lattice parameters $a = 0.301$ nm, $b = 0.382$ nm and $c = 0.826$ nm, staked along *c*-axis, that can be described by a *Pmmn* space group.

Thermal stability of the orthorhombic structure of titania nanotubes depended on annealing atmosphere and temperature. In a N_2 atmosphere, the structure transformed into anatase at 250 °C while in air the structure transformed at 400 °C. During annealing the nanotubular structure releases hydroxyls and Ti^{4+} cations are self-reduced into Ti^{3+} forming an oxygen deficient non-stoichiometric anatase phase, which eventually collapse the nanotubular morphology. The self-reduction process of Ti^{4+} cations is enhanced when the annealing treatment is done in N_2 atmosphere rather than in air, yielding highly oxygen-deficient anatase nanoparticles on the nanotubes walls.

References

[1] N. Sakai, Y. Ebina, K. Takada, T. Sasaki, J. Am. Chem. Soc. 126 (2004) 5851.
[2] C. Drew, X. Liu, D. Ziegler, X. Wang, F.F. Bruno, J. Whitten, L.A. Samuelson, J. Kumar, Nano Lett. 3 (2003) 143.
[3] S. Ushiroda, N. Ruzycki, Y. Lu, M.T. Spitler, B.A. Parkinson, J. Am. Chem. Soc. 127 (2005) 5158.
[4] L. Feng, Y. Liu, J. Hu, Langmuir 20 (2004) 1786.
[5] S. Dzwigaj, C. Luis, M. Breysse, M. Cattenot, V. Bellière, C. Geantet, M. Vrinat, P. Blanchard, E. Payen, S. Inoue, H. Kudo, Y. Yoshimura, Appl. Catal. B 41 (2003) 181.
[6] M. Breysse, J.L. Portefaix, M. Vrinat, Catal. Today 10 (1991) 489.
[7] J. Ramirez, L. Cedeño, G. Busca, J. Catal. 184 (1999) 59.
[8] S. Inoue, A. Muto, H. Kudou, T. Ono, Appl. Catal. A 269 (2004) 7.
[9] H. Wang, Y. Wu, B.-Q. Xu, Appl. Catal. B: Environ. 59 (2005) 139.
[10] U. Diebold, Surf. Sci. Rep. 48 (2003) 53.
[11] X. Bokhimi, A. Morales, M. Aguilar, J.A. Toledo Antonio, F. Pedraza, Int. J. Hydrogen Energy 26 (2001) 1279.
[12] S. Inoue, A. Muto, T. Ono, T. Makabe, T. Takatsuka, H. Nomura, US2004/0238410 A1.
[13] T. Kasuga, M. Hiramatsu, A. Hoson, T. Sekino, K. Niihara, Langmuir 14 (1998) 3160.
[14] G.H. Du, Q. Chen, R.C. Che, Z.Y. Yuan, L.M. Peng, Appl. Phys. Lett. 79 (2001) 3702.
[15] R. Tenne, Nature 431 (2004) 640.
[16] R. Tenne, Angew. Chem. Int. Ed. 42 (2003) 5124.
[17] C. Cheng, H. Teng, Chem. Mater. 16 (2004) 4352.
[18] J. Escobar, J.A. Toledo, M.A. Cortés, M.L. Mosqueira, V. Perez, G. Ferrat, E. López Salinas, E. Torres, Catal. Today 106 (2005) 222.
[19] Q. Chen, G.H. Du, S. Zhang, L.M. Peng, Acta Cryst. B 58 (2002) 587.
[20] Q. Cheng, W. Zhou, G. Du, L.M. Peng, Adv. Mater. 14 (2002) 1709.
[21] J. Yang, Z. Jin, X. Wang, W. Li, J. Zhang, S. Zhang, X. Guo, Z. Zhang, Dalton Trans. (2003) 3898.
[22] R. Ma, Y. Bando, T. Sasaki, Chem. Phys. Lett. 380 (2003) 577.
[23] R. Ma, K. Fukuda, T. Sasaki, M. Osada, Y. Bando, J. Phys. Chem. B 109 (2005) 6210.
[24] M. Sugita, M. Tsuji, M. Abe, Bull. Chem. Soc. Jpn. 63 (1990) 1978.
[25] C.C. Tsai, H. Teng, Chem. Mater. 18 (2006) 367.
[26] T. Sasaki, M. Watanabe, H. Hashizume, H. Yamada, H. Nakazawa, J. Am. Chem. Soc. 118 (1996) 8329.
[27] Y.V. Kolen'ko, K.A. Kovnir, A.I. Gavrilov, A.V. Garshev, J. Frantti, O.I. Lebedev, B.R. Churagulov, G.V. Tendeloo, M. Yoshimura, J. Phys. Chem. B. 110 (2006) 4030.
[28] M. Hodos, E. Horváth, H. Haspel, A. Kukovecz, Z. Kónya, I. Kiricsi, Chem. Phys. Lett. 399 (2004) 512.
[29] A. Kukovecz, M. Hodos, Z. Kónya, I. Kiricsi, Chem. Phys. Lett. 411 (2005) 445.
[30] D.V. Bavykin, J.M. Friedrich, A.A. Lapkin, F.C. Walsh, Chem. Mater. 18 (2006) 1124.
[31] S. Xie, E. Iglesia, A. Bell, J. Phys. Chem. B 105 (2001) 5144.
[32] http://srdata.nist.gov/xps/.
[33] S. Hashimoto, A. Murata, T. Sakurada, A. Tanaka, J. Surf. Anal. 9 (2002) 459.
[34] X. Chen, C. Burda, J. Phys. Chem. B. 108 (2004) 15446.
[35] H. Berger, H. Tang, F. Lévy, J. Cryst. Growth 130 (1993) 108.
[36] S. Brunauer, L.S. Deming, W.E. Deming, E. Teller, J. Am. Chem. Soc. 38 (1940) 1723.
[37] V. Idakieva, Z.-Y. Yuanb, T. Tabakovaa, B.-L. Sub, Appl. Catal. A 281 (2005) 149.
[38] R. Ma, T. Sasaki, Y. Bando, J. Am. Chem. Soc. 126 (2004) 10382.